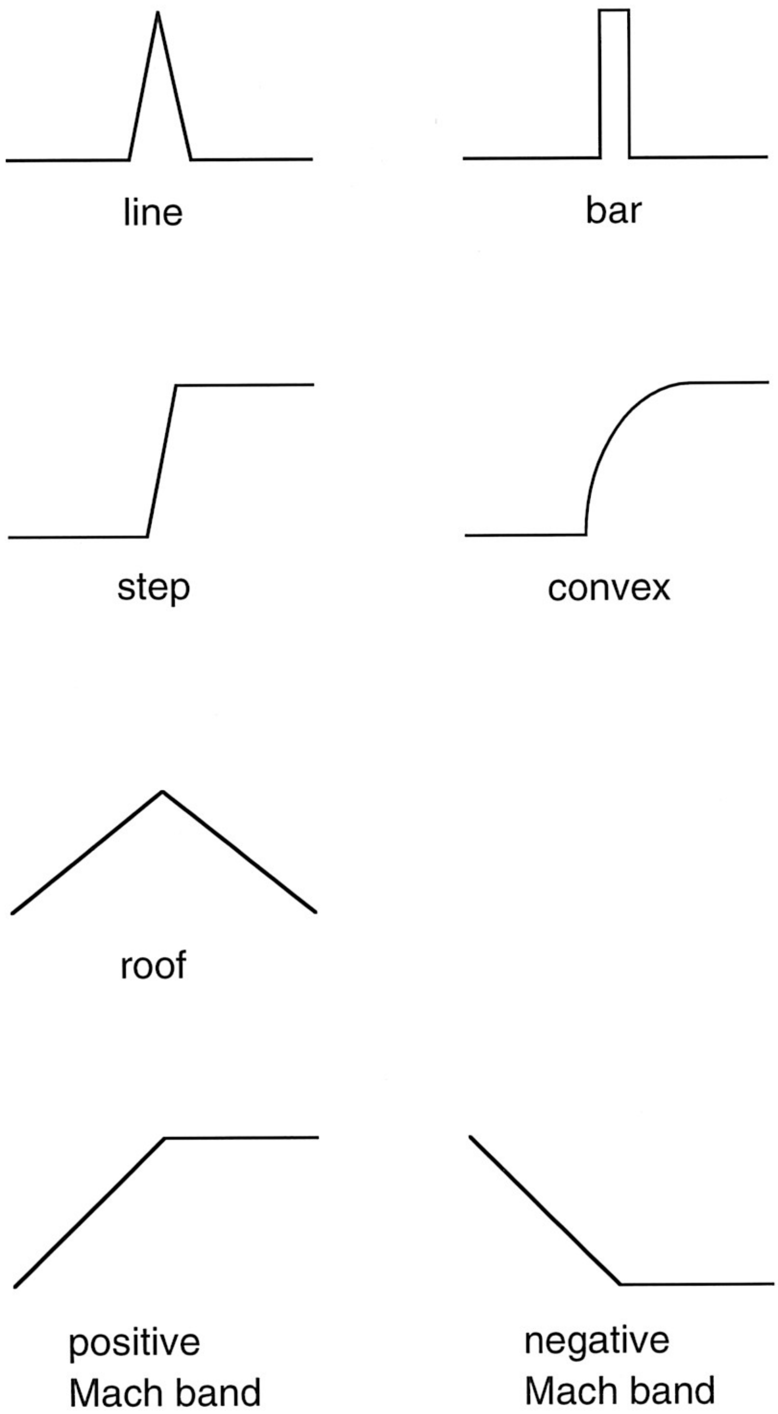


**Figure 1.** Grey-level profiles (across the normal direction) of seven primary types of edges.

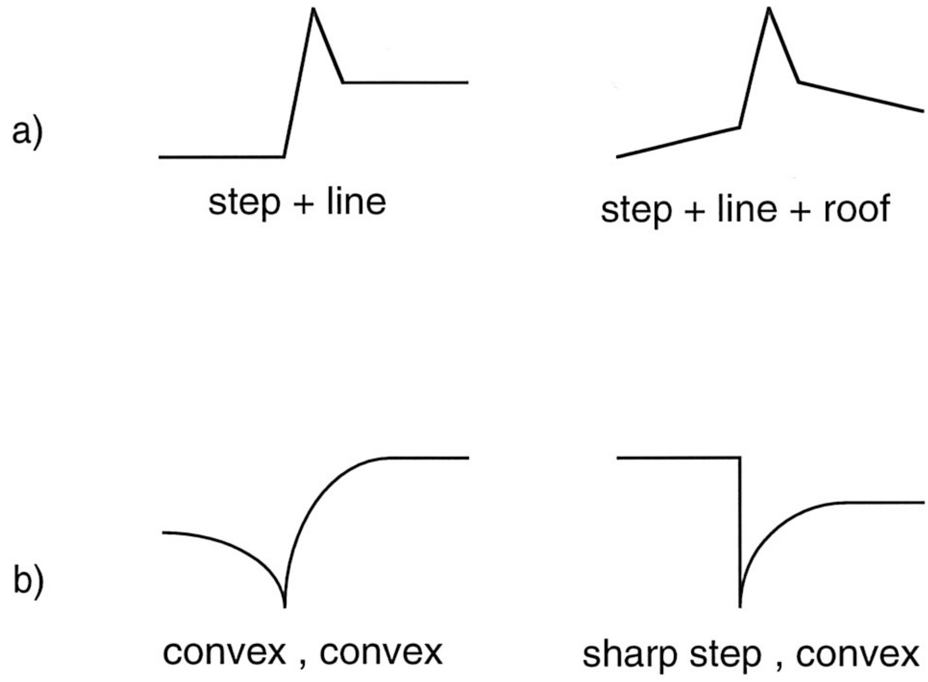


**Figure 2.** Secondary types of edges can be built by combining edges of primary type in two ways: a) linear superposition; b) succession. We show in both cases the grey-level profiles across the normal direction.

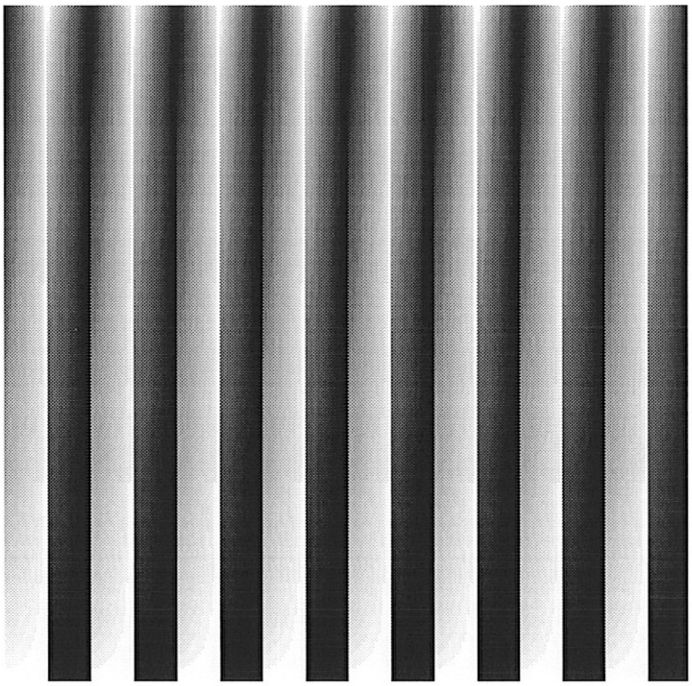

**Figure 3**. Vertical grating whose horizontal sections are varying from a triangular wave to a square one. In the middle, where both waves are superposed, the edges (combining a step and a roof) are seen slightly to the left of their true location. This is consistent with the phase congruence model for the human perception of edges.

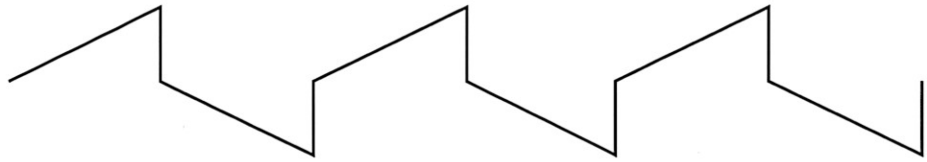

**Figure 4.** Grey-level profile across a horizontal line in the middle of Figure 3.

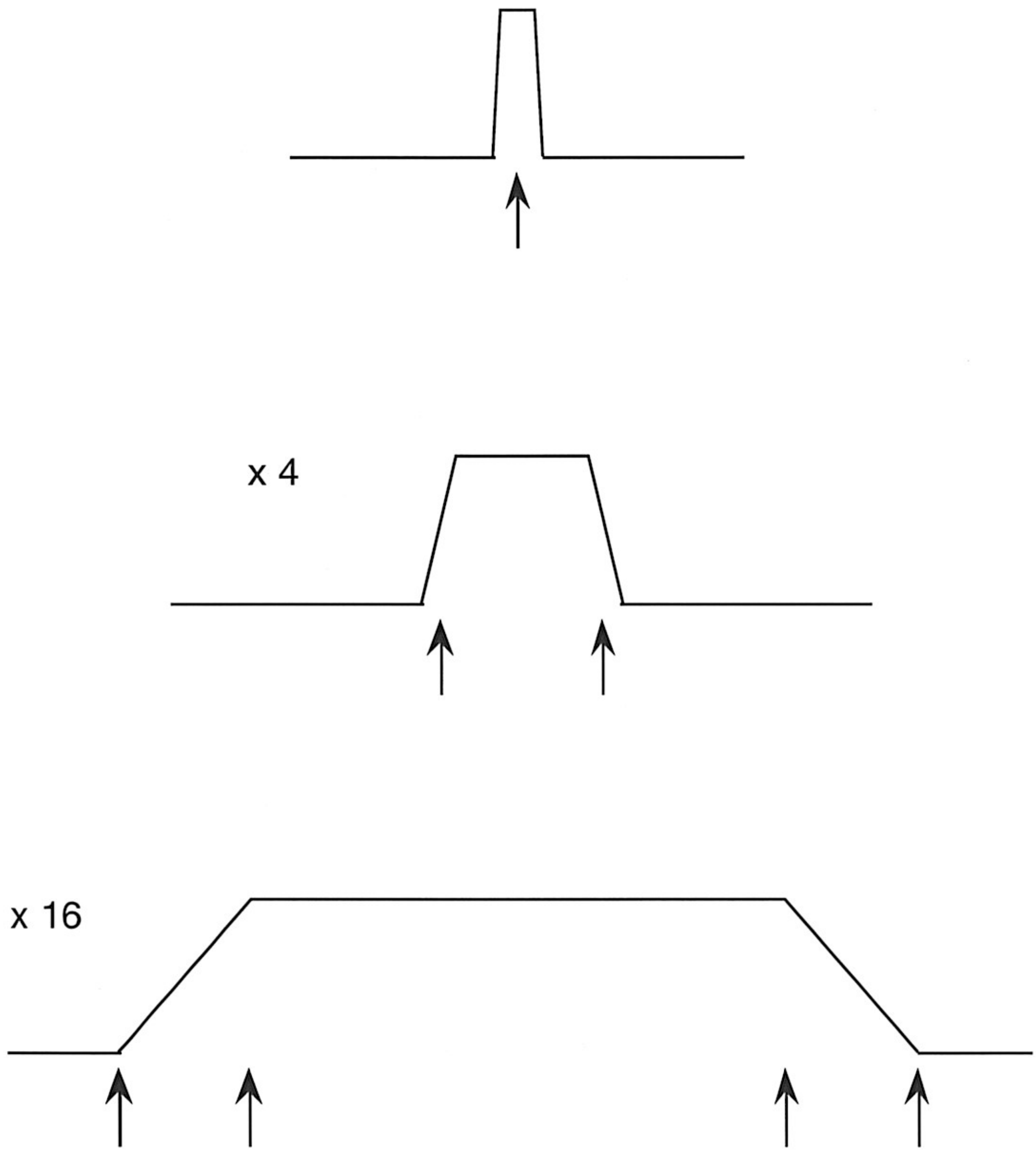


**Figure 5.** A bar edge profile shown in its original size, then magnified 4 times, and finally 16 times. Arrows indicate the position of edges at each scale.

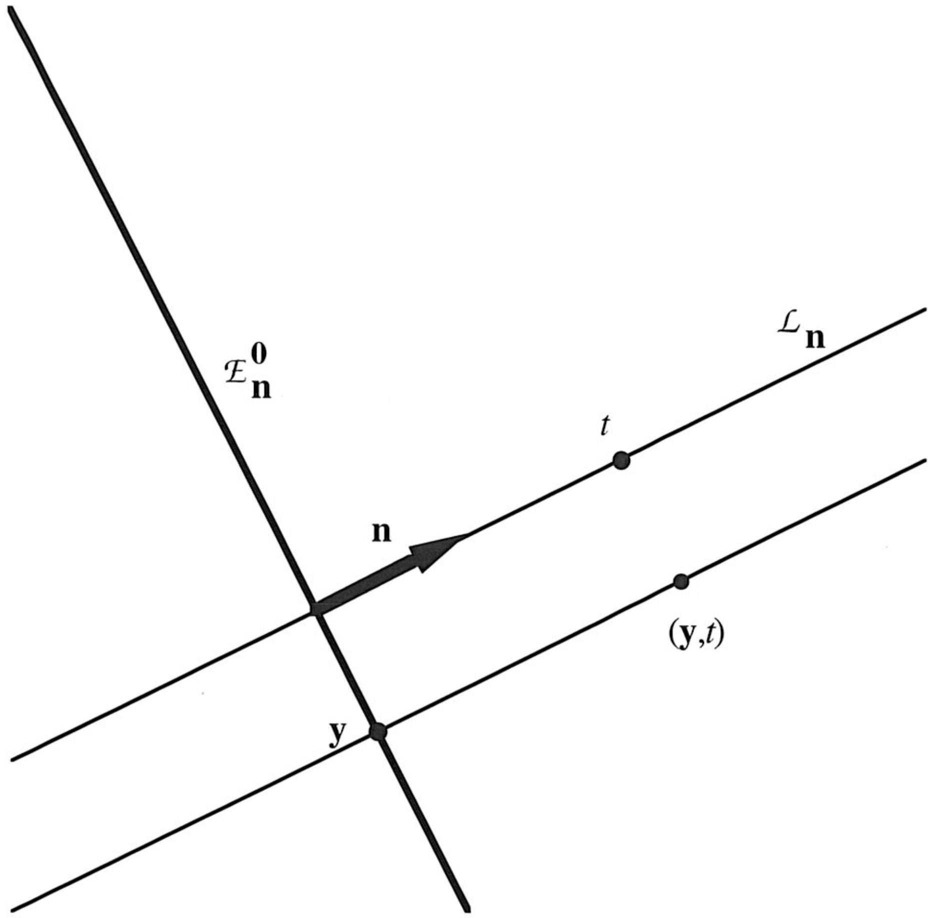


**Figure 6.** Decomposition of $\mathbf{x} \in \mathcal{E}$ into $(\mathbf{y},t) \in \mathcal{E}_{\mathrm{n}}{}^{0} \times \mathbb{R}$.

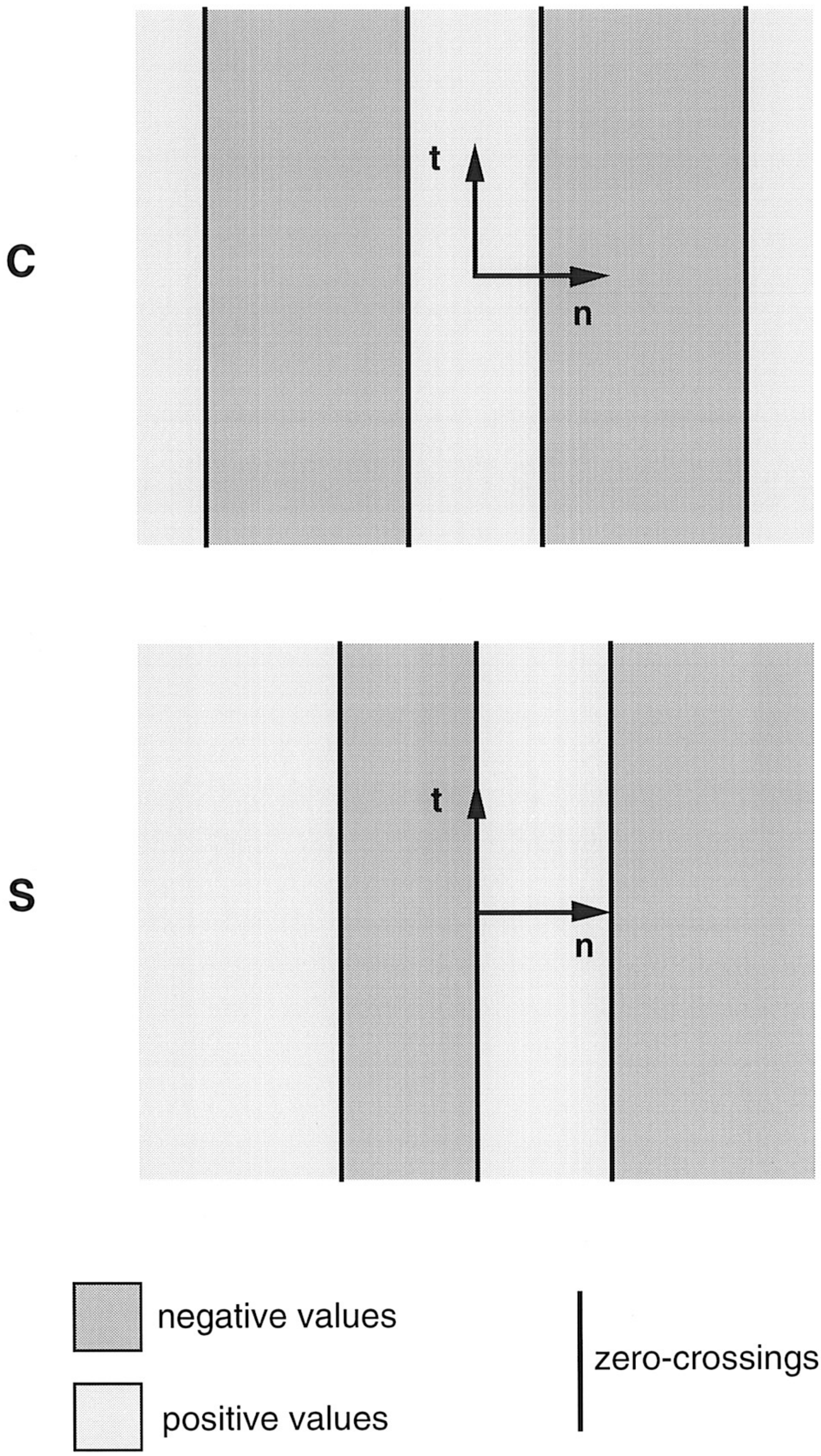


**Figure 7.** Typical pattern for the signs taken by the values of the two filters.

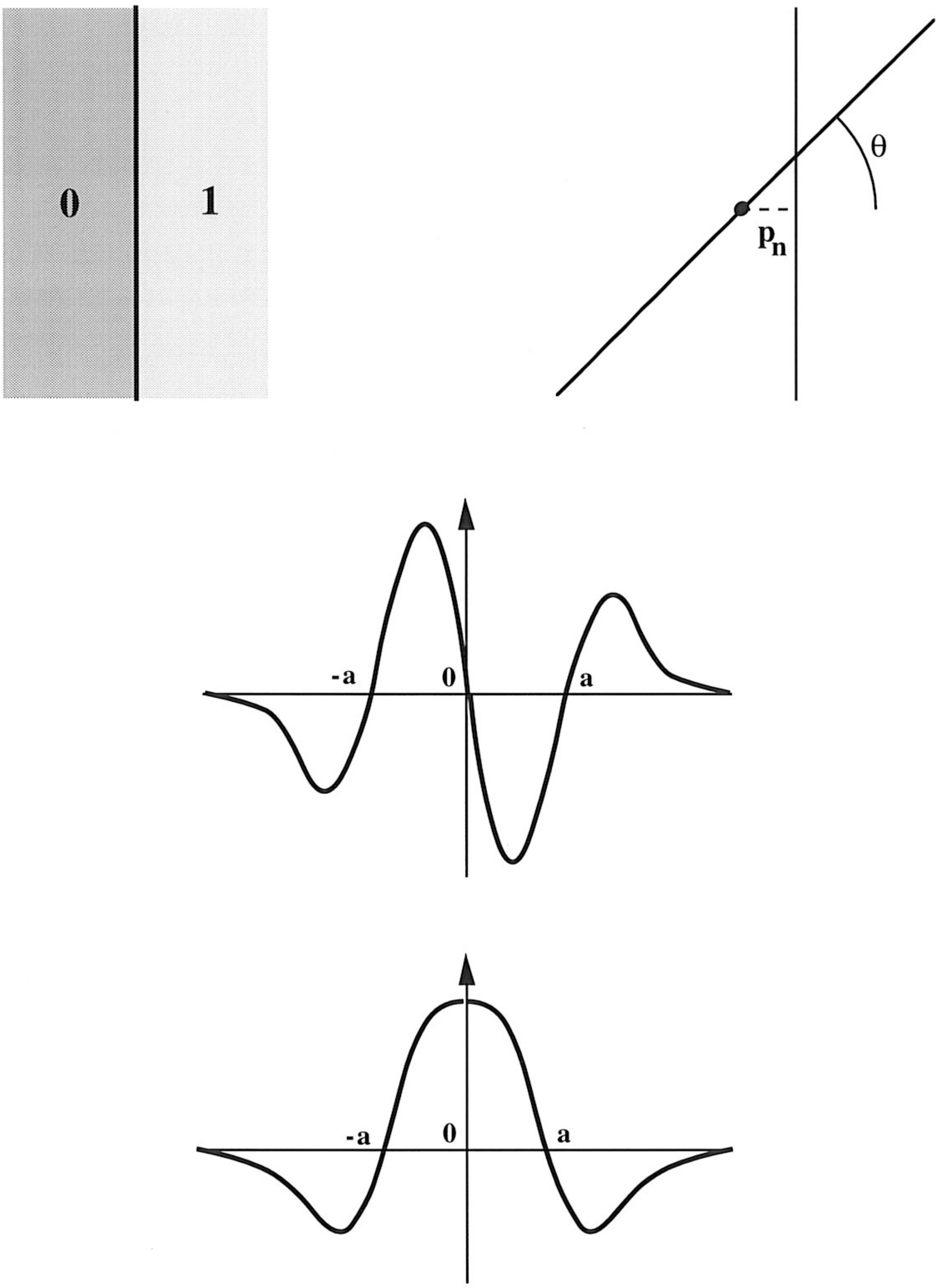


**Figure 8.** Top left: two-dimensional Heaviside step edge. Top right: geometrical illustration of the convolution of $F_\theta$ by the Heaviside step edge, calculated at a point $\mathbf{p} = (p_t,p_n)$ Below: two possible profiles for the function $f$, one even-symmetric and the other odd-symmetric.

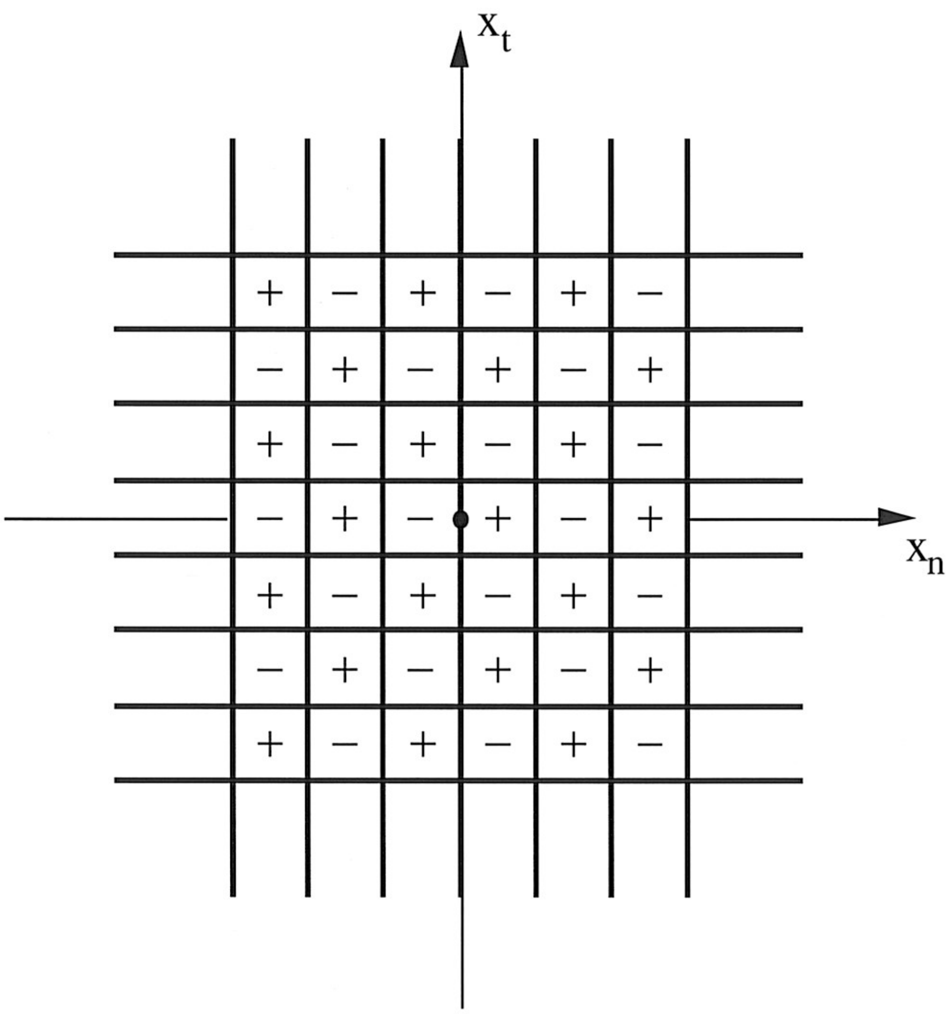


**Figure 9.** Signs and zero-crossings of the function $F$ (the product of a Gabor sine function in the normal direction and a Gabor cosine function in the tangential direction) given in (4.38).

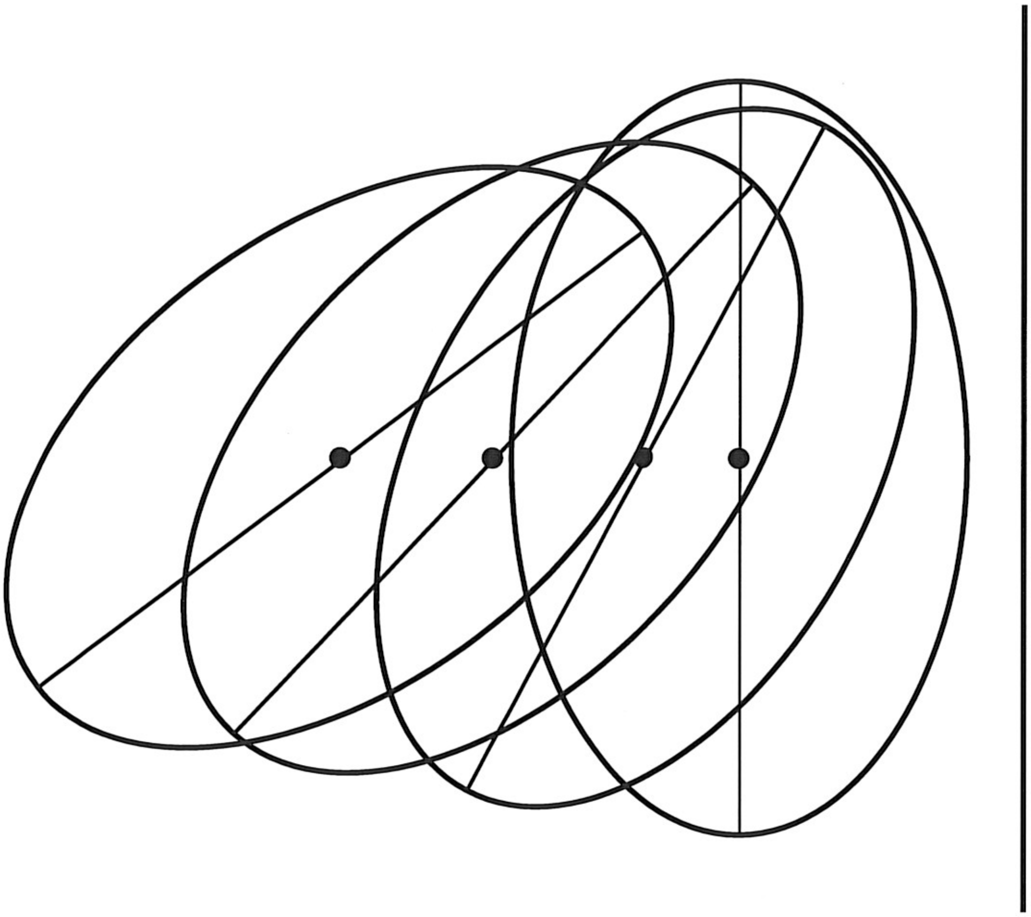

**Figure 10.** Choose the Gaussian derivative filter given in (4.43) with $\tau = 5$ and $\nu = 3$. The support of the filter is represented by an ellipse with great axis $\tau$ and small axis $\nu$, where we show the long axis (corresponding to the tangential axis, which is the locus of zero-crossings of the filter). Orientation selectivity holds for points at distance $p \leq 3.75$ from the true edge position. We show the support of the filter rotated by the angle $\theta_p$ given by (4.49), for which the energy function is highest, for the values $p = 3.75$ ($\theta_p = 0°$), $p = 5$ ($\theta_p = 27.88°$), $p = 7$ ($\theta_p = 43.40°$), $p = 9$ ($\theta_p = 52.62°$).

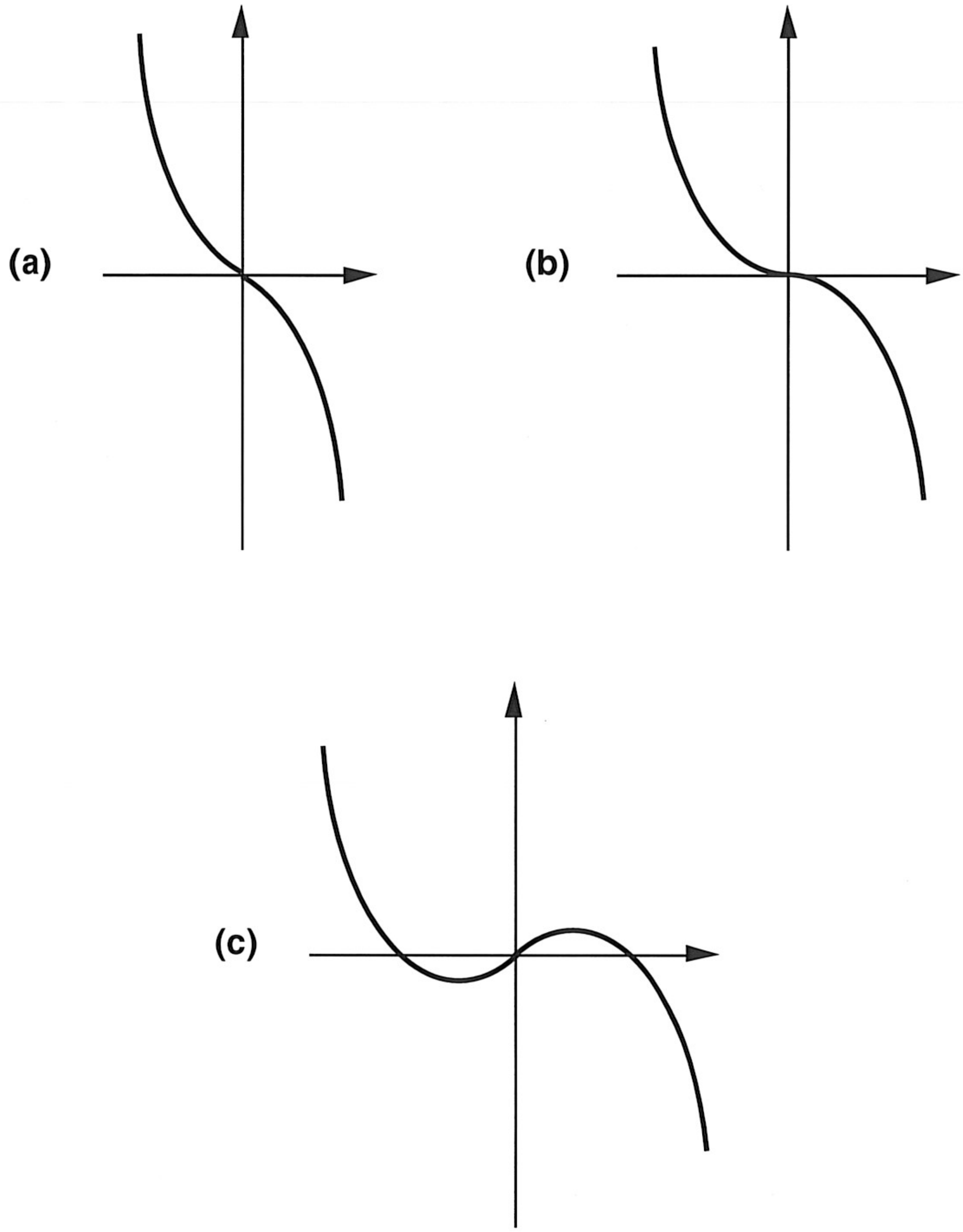


**Figure 11.** As the scale increases from (a) to (c), a non-causal local maximum of the energy function is created.

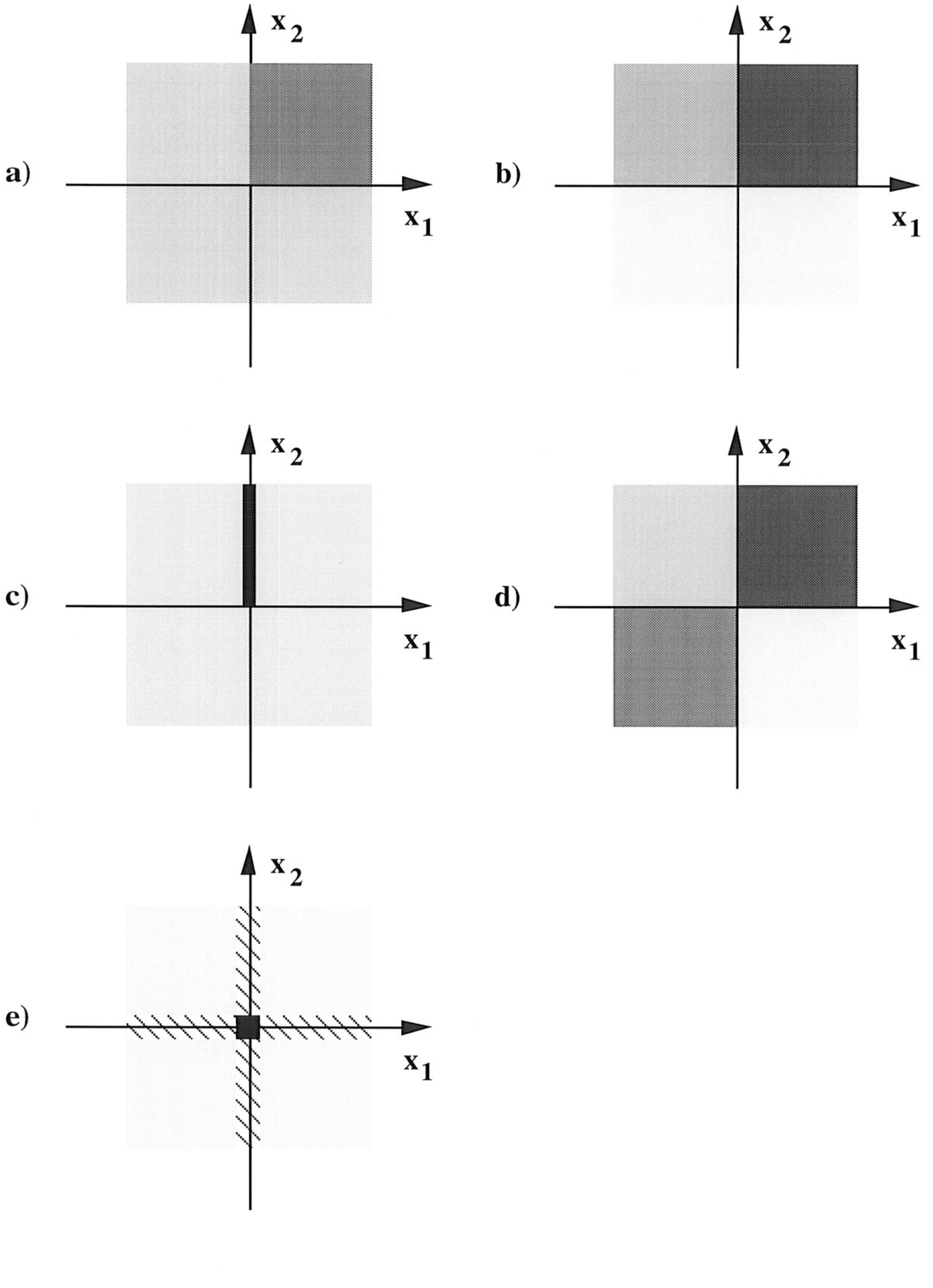


**Figure 12.** Some types of bi-directional features: a) a corner; b) a T-junction; c) a line termination; d) an X-junction; e) a peak (or blob).

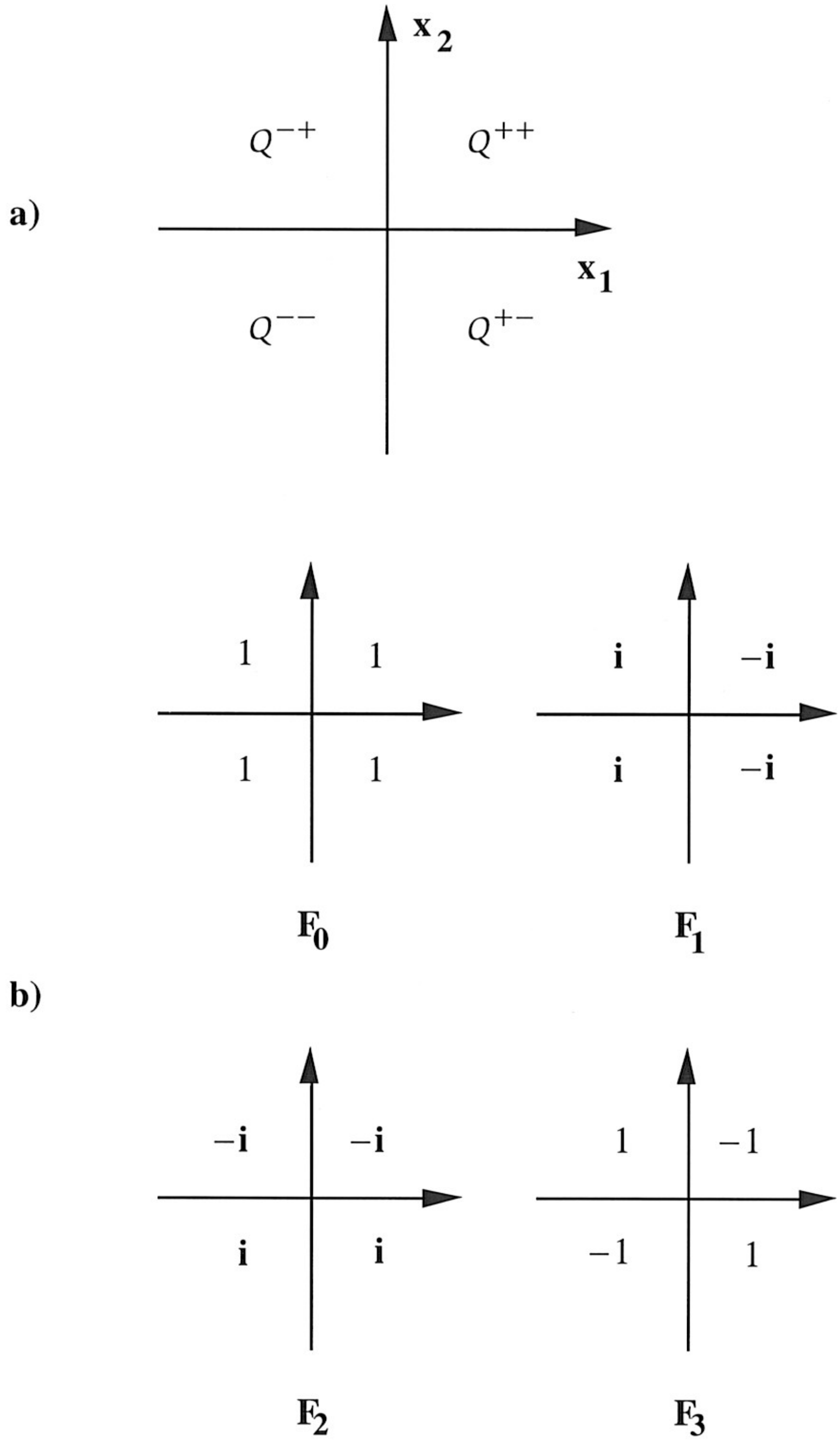


**Figure 13.** a) The four quadrants. b) The sign of the Fourier transforms of the four filters in each of the four quadrants.

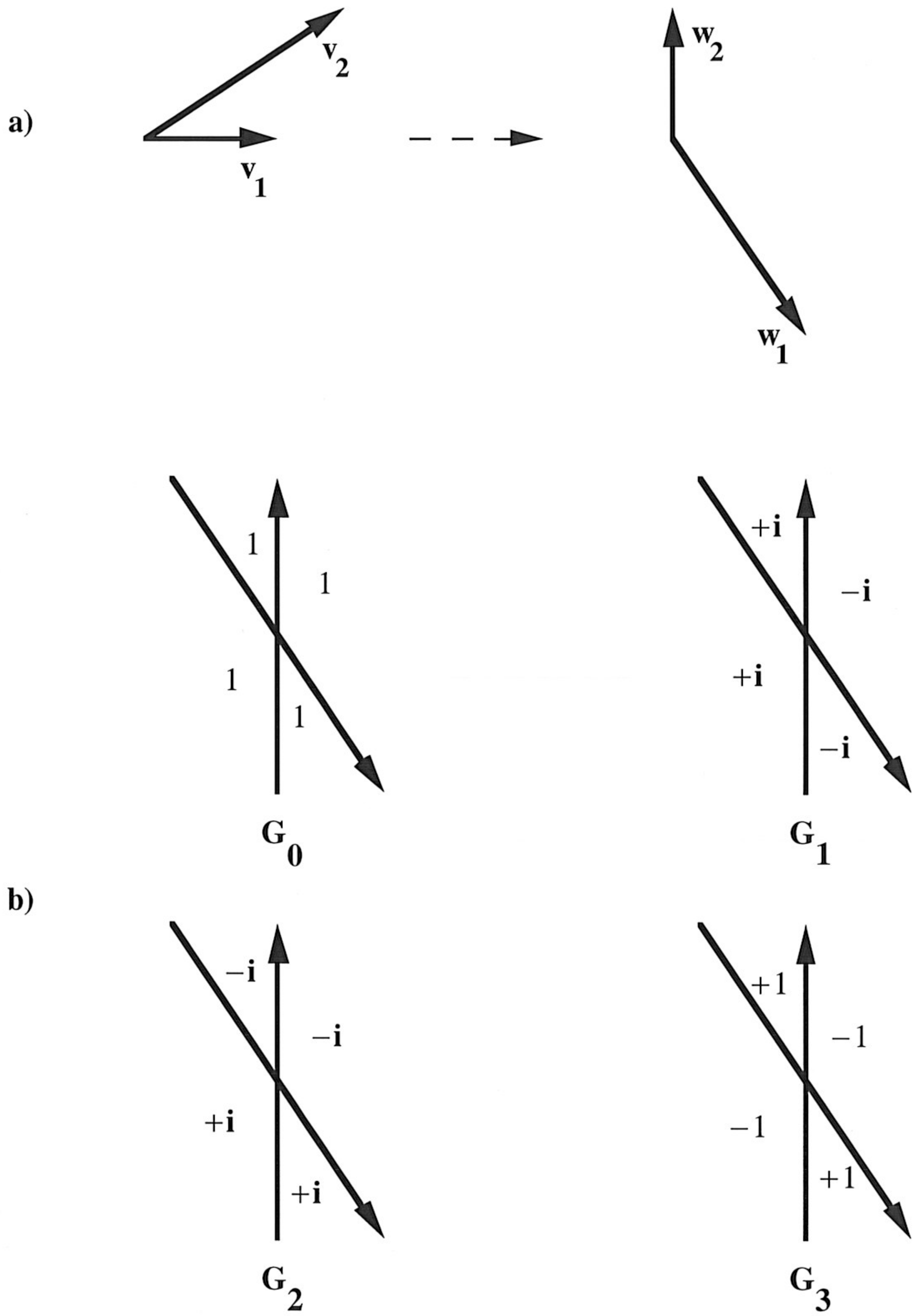


**Figure 14.** a) We derive from the basis $\{v_1, v_2\}$ the conjugate basis $\{w_1, w_2\}$. b) The four filters $G_0$, $G_1$, $G_2$, and $G_3$ oriented along the basis $\{v_1, v_2\}$ have their Fourier transforms whose signs are constant in the four quadrants determined by $w_1$ and $w_2$, shown here.

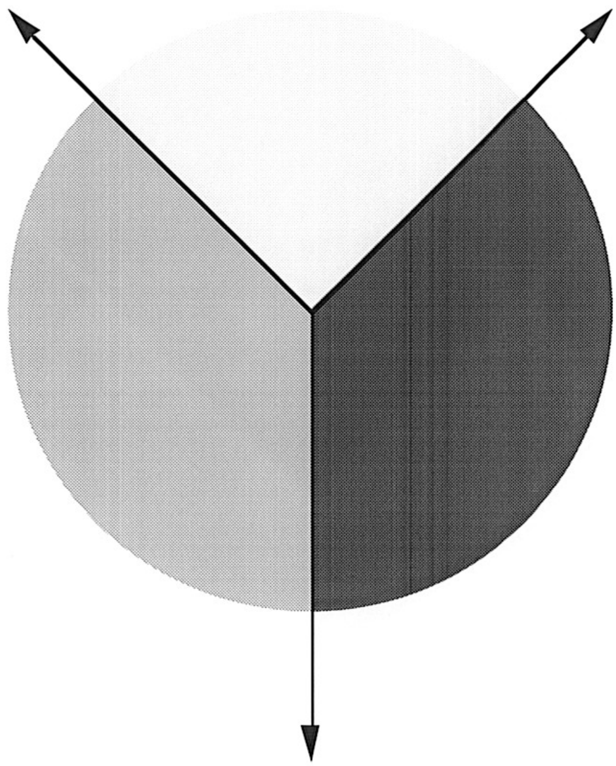

**Figure 15.** A Y-junction is a tri-directional feature which does not correspond to the model described in Subsection 5.2